International Journal of Microwave and Wireless Technologies

cambridge.org/mrf

Millimeter-wave wideband high-gain LTCC phased array antenna based on ridged substrate integrated waveguide

Sha Xu[1], Guiping Jin[2], Dujiao Lu[2] and Shaowei Liao[2]

[1]School of Integrated Circuits, Guangdong University of Technology, Guangzhou, China and [2]School of Electronic and Information Engineering, South China University of Technology, Guangzhou, China

Research Paper

Cite this article: Xu S, Jin G, Lu D, Liao S (2025) Millimeter-wave wideband high-gain LTCC phased array antenna based on ridged substrate integrated waveguide. *International Journal of Microwave and Wireless Technologies* **17**(4), 642–652. https://doi.org/10.1017/S1759078725000534

Received: 14 September 2024
Revised: 15 April 2025
Accepted: 19 April 2025

Keywords:
Millimeter-Wave (mmWave); Phased Array; Ridged Substrate Integrated Waveguide (RSIW); 5G

Corresponding author: Guiping Jin;
Email: gpjin@scut.edu.cn

Abstract

In this paper, a millimeter-wave (mmWave) wideband high-gain low-temperature co-fired ceramic (LTCC) phased array using ridged substrate integrated waveguide (RSIW) element is proposed, which can cover n257/n258 bands (24.25–29.5 GHz). First, a novel widebeam and high-gain RSIW slot antenna subarray is designed, which is constructed by staggered longitudinal slot that incorporated with additional radiating elements on the non-scanning plane. Further, the proposed widebeam antenna subarray is applied to construct a 1 × 4 array integrated in an LTCC package with small element spacing of about $0.41\lambda_0$. Moreover, by adding isolation slots and metal vias between adjacent array elements, the isolation of ports thereby is reduced below −15 dB, and the scanning range is increased up to ±7°. A wideband and low-loss feeding network is realized by series-parallel combined feeding, further improving isolation and scanning performance after assembly. The simulation and measurement demonstrate that the antenna array possesses satisfied beam-scanning capabilities over wide bandwidth of ∼20%, achieving maximum scanning angle up to ±62° while maintaining desirable gain above 14.5 dBi. Furthermore, within the entire operating bandwidth, the scanning angles extend to ±55° with minimal variation. These features show that the proposed antenna array is promising for 5G mmWave communications.

Introduction

The 5 G millimeter-wave (mmWave) technology has captured significant interest due to its large bandwidth and high data rate [1–3]. Regarding the inherent transmission loss in air is negligible under mmWave band, phased arrays become one of the key technologies, and have attracted the extensive attention. Phased arrays have more flexible beam pointing and strong anti-interference performance; therefore, phased arrays are widely employed to attain dynamic point-to-point high data rate wireless communication [4–6]. In this circumstance, the phased arrays with the ability of wide-angle scanning, wideband, high-gain characteristics, as well as compact sizes are highly required.

There are many types of antennas that can achieve wide-angle scanning performance, such as electromagnetic dipoles, substrate integrated waveguide (SIW) horn antennas, patch antennas, SIW/ridged substrate integrated waveguide (RSIW) slot antennas, planar inverted-F antenna antennas, etc. However, since the mutual coupling between the array elements becomes stronger with the scanning angle increases, the wide-angle scanning performance is still limited by mutual coupling nowadays [7]. Among different type of antennas, RSIW slot antennas combine the advantages of ridge waveguides and SIW together [8, 9]. RSIW slot antennas have lower cutoff frequency of the dominant mode and wider single-mode operating bandwidth [10]. In terms of fabrication feasibility and cost, RSIW slot antennas have lower cost compared to ridge waveguides and are easier to integrate with planar circuits. Compared to SIW slot antennas, RSIW slot antennas have advantages of wider bandwidth, lower sidelobe, and smaller size [11]. Furthermore, adjustable ridge dimensions can minimize the waveguide width, which theoretically can make the scanning angle reach ±90° without generating grating lobes [12, 13]. However, though the advantage of RSIW slot antenna is obvious, it still has some technical challenge to solve. The RSIW slot antenna is resonant antenna, which typically have narrow bandwidth. Furthermore, due to the internal dielectric materials inside and low profiles, the mutual coupling between array elements is extensive, which has adverse influence on the impedance bandwidth and gain.

Many methods have been used to improve the impedance bandwidth and gain of phased arrays. Common approaches to solving bandwidth issues include adding new resonance points, designing wideband feeding networks, and dividing the antenna into multiple subarrays.

© The Author(s), 2025. Published by Cambridge University Press in association with The European Microwave Association.

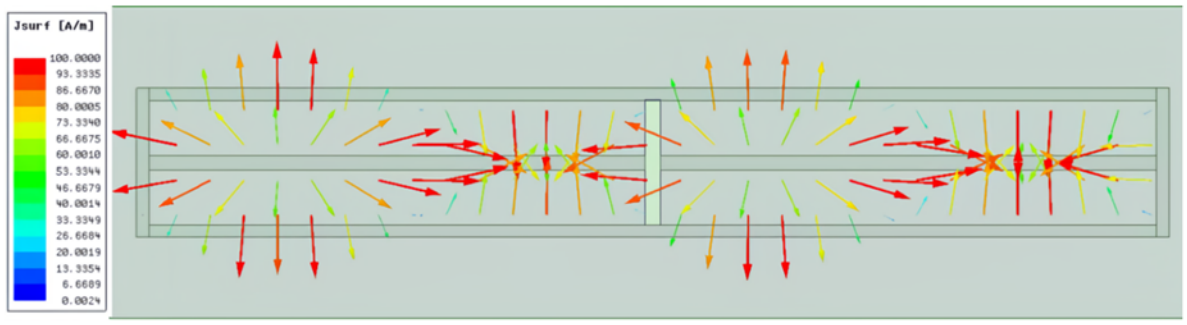


Figure 1. Surface current distribution of RSIW slot.

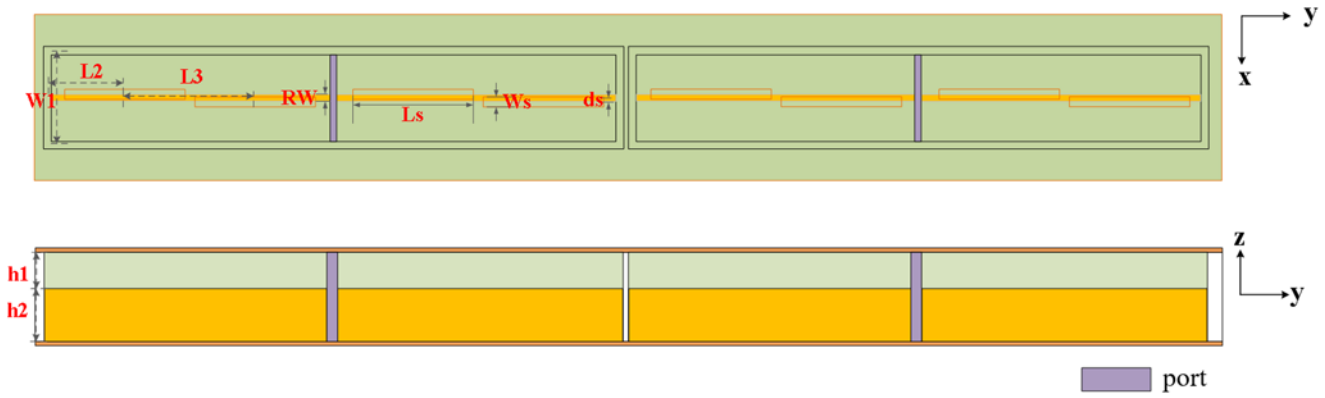


Figure 2. Top and side views of the RSIW slot antenna subarray.

Methods to improve antenna gain include increasing the physical area of the radiation aperture, enhancing directionality to achieve uniform E-field distribution on the aperture surface, and reducing losses to improve radiation efficiency. For instance, in paper [14], a dual-polarized SIW cavity-backed coupling fed slot element antenna was proposed. It employed to design a 1 × 4 phased array that covers the frequency range of 25.8–28.8 GHz (11%), and has a scanning range greater than ±41°. In paper [15], an open-ended cavity structure was employed, giving rise to a compact 4 × 4 end-fire phased array, attaining a wide bandwidth of 24.5–29.5 GHz (18.5%) and a scanning range greater than ± 46°. In paper [16], an end-fire phased array for 5 G (27.5–29.5 GHz, 7%) handset devices was proposed, and scanning range of ±44° was achieved by introducing two transition plates to improve the impedance matching. In paper [17], the proposed phased array showed a realized gain above 6 dBi within the frequency of 28–33 GHz (13%) and achieve beam-steering up to ±40°. In paper [18], a low-cost and low-profile magnetic actuator is introduced to precisely control the phase shifter, and the phased array achieves the bandwidth of 29.5–30.5 (3.3%) and scanning range of ±38°.

However, as mentioned above, most reported mmWave phased-arrays have limited bandwidth, scanning range and the gain. To meet the requirements of mmWave 5 G (24.25–29.5 GHz) standards, a novel wideband and high-gain phased array antenna based on low-temperature co-fired ceramic (LTCC) technology is proposed in this paper for wide-angle scanning. The verification results show that the phased array can obtain a good beam-scanning capability covering a large bandwidth of ∼20%, the scanning angles extend up to ±55° covering the entire bandwidth of 24.25–29.5 GHz. The isolation of ports remain below −15 dB and the gain over 14.5 dBi with minimal variations.

Design of RSIW slot antenna subarray

The type of antenna subarray is a slot antenna based on RSIW. The proposed subarray consists of two parts: the radiator and the feeder. The radiator comprises several staggered longitudinal slots on the RSIW. The feeder comprises a T-junction power divider feeding RSIW through slot coupling, and the feeder transit from ground coplanar waveguide (GCPW) to (SIW. LTCC technology is employed in this design, since it can offer arbitrary inter-layer via, offering higher design flexibility compared to standard Printed Circuit Board (PCB)/ High-Density Interconnect (HDI) process.

Design of element RSIW slot antenna

The relative height between the ridge and waveguide significantly impacts overall performance of the RSIW slot antenna. As observed from the simulation. For the ridge height h_2, when the ridge height increases, it will reduce the cutoff frequency of some modes, thereby increasing the difference in cutoff frequencies between different modes, and thus expanding the single-mode transmission bandwidth. By adjusting the ridge height h_2, the operating frequency range of the antenna can be extended. Therefore, the ridge height should be optimized well to achieve the broader bandwidth and higher gain. The working principle of RSIW is similar to SIW, which can be observed from the surface current distribution in Figure 1. The staggered longitudinal slots along the center line of the wide side are cut by the current distribution lines, then the displacement currents can be generated on both sides of the slots, where electromagnetic waves can be excited. This current distribution specifies the level of power coupled from the waveguide to the slot and consequently radiation from the slot. The

https://doi.org/10.1017/S1759078725000534 Published online by Cambridge University Press

Table 1. Dimension parameters of the RSIW slot radiation element

Parameters	Value (mm)	Parameters	Value (mm)
L_2	1.9	L_3	3.8
h_1	0.282	h_2	0.47
RW	0.23	L_s	3.7
W_s	0.3	d_s	0.11
W_1	2.22		

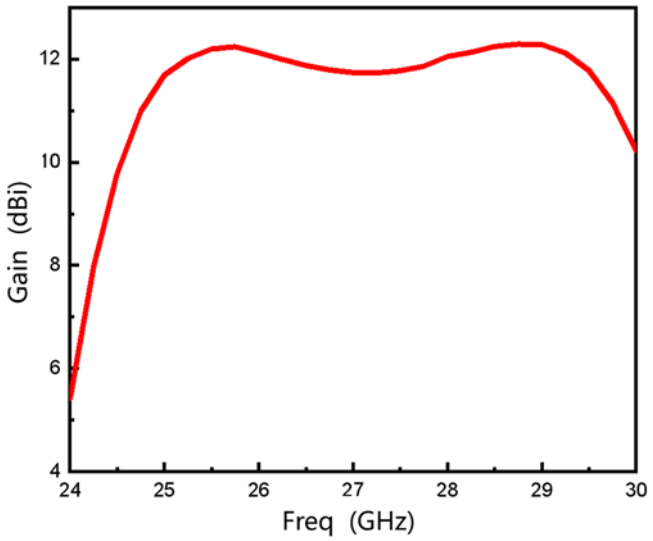


Figure 3. Simulated gain of the RSIW slot antenna subarray.

cutting directions of each slot should be consistent, to ensure the electric field are in the same polarization, which can maximize the aperture efficiency. In initial simulation, the complex metallized via model is transformed into an equivalent metal wall to save the simulation cost.

The radiators are implemented on an eight-layer LTCC dielectric substrate, since it has higher dielectric constant, which can make the size more compact. The LTCC process utilized in this design is FerroA6M ($\varepsilon_r = 5.9$, $\tan\delta = 0.002$), and the single-layer substrate thickness is 0.094 mm. To achieve higher gain, eight slots are set as radiation elements, which are further divided into two subarrays to form the radiator. The topmost metal layer is etched with eight staggered longitudinal placed radiation slots along the center line of the wide side, each with a length of L_s and a width of W_s. The length from the slot to the short-circuit end is L_2, the offset from the center line is d_s, and the spacing between adjacent slots is L_3. The top and side views of the antenna subarray are shown in Figure 2.

It was found that due to the strong electric field above the ridge, the offset of the slot from the center line (d_s) has a significant impact on radiation performance. As observed from the simulation, when the slot deviates from the center line, the electric field distribution around the slot is disrupted, and can cause the main beam direction to shift. When the slot is offset toward one side, the radiation pattern may be tilted towards the opposite side. When the slots are too far from the center line, it may cause the antenna to become more capacitive or inductive, leading to impedance mismatches, result in increased return loss and voltage standing

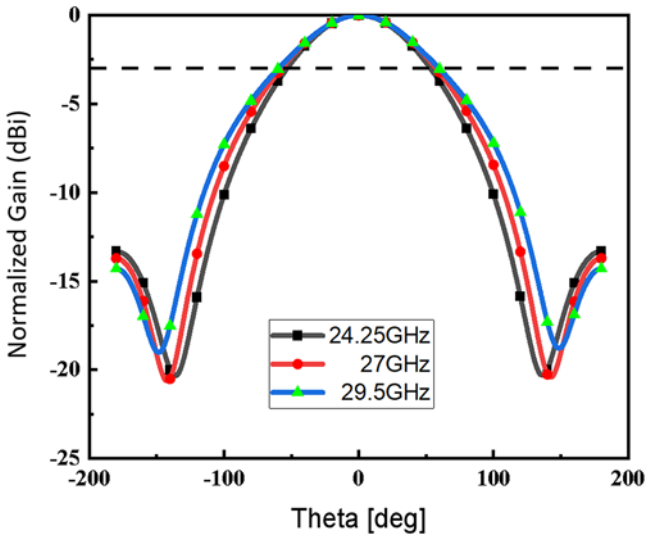


Figure 4. Normalized radiation patterns of the RSIW slot antenna subarray at 24.25, 27, and 29.5 GHz.

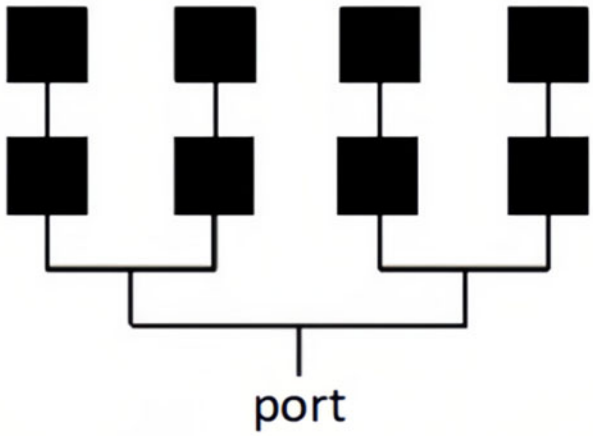


Figure 5. Schematic diagram of series-parallel feeding network.

wave ratio (VSWR). The length from the slot to the short-circuit end (L_2) and the spacing between adjacent slots (L_3) mainly affect impedance matching. Additionally, the ridge width (RW) and ridge height also have impact on matching. The higher height can easily result in higher-order mode, while the lower height can cause waveguide cutoff. After optimization, the specific dimension values are presented in Table 1.

The ports of the two subarrays are excited by equal amplitude and anti-phase excitation. The gain within the operating band is shown in Figure 3. It can be seen that the gain is above 11 dBi at most frequencies with minimal variation. Figure 4 shows the normalized radiation patterns at different frequencies. The half-power beamwidth of the radiator is above 106° within the operating band. The minimum beamwidth is 106° at the low-frequency point of 24.25 GHz, and the maximum beamwidth is 125° at the high-frequency point of 29.5 GHz. The radiation performance demonstrated by this radiator is desirable, meeting the scanning requirements of 5 G-mmWave phased array.

https://doi.org/10.1017/S1759078725000534 Published online by Cambridge University Press

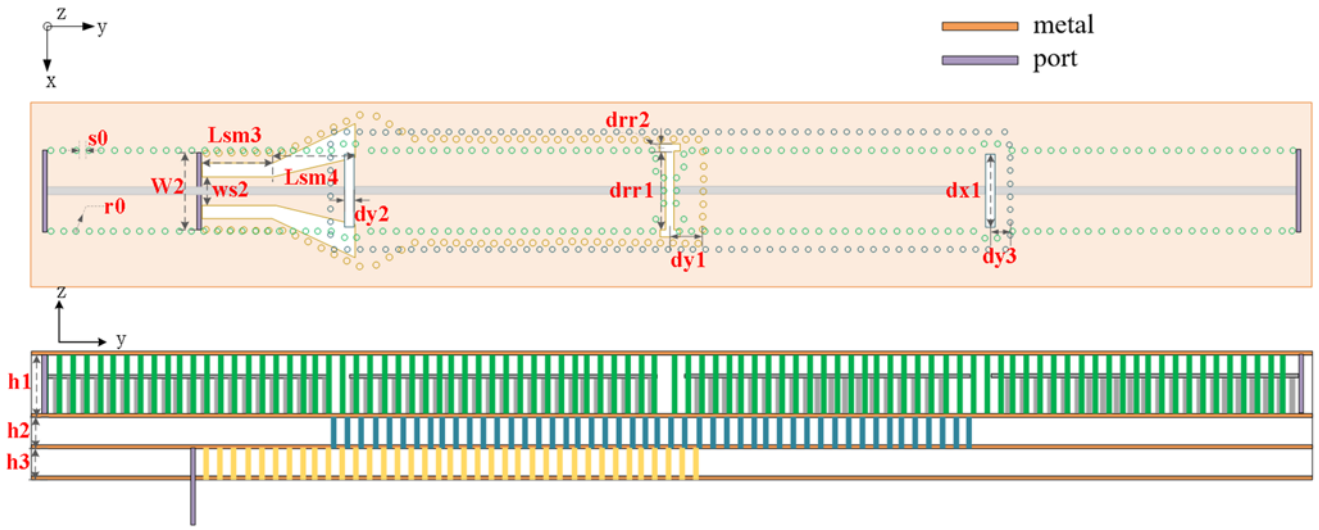


Figure 6. Schematic diagram of SIW-fed RSIW.

Table 2. Dimension parameters of the feeding network

Parameters	Value (mm)	Parameters	Value (mm)
W_2	1.545	h_3	0.47
h_2	0.47	s_0	0.35
W_{s2}	0.74	r_0	0.17
d_{y1}	0.736	d_{rr1}	2.29
L_{sm3}	2.13	d_{rr2}	0.204
L_{sm4}	2.7	d_{x1}	2.1
h_1	0.752	d_{y2}	0.324
d_{y3}	0.406		

Design of series-parallel feeding network

The feeding network adopts series-parallel combined feeding approach; the diagram is illustrated in Figure 5. This approach ensures consistent path lengths from the excitation source to each radiator section, where a single coupling path sequentially feeds multiple radiator elements. This approach combines the advantages of both series and parallel feeding, achieving both broadband and low-loss characteristics. As depicted in Figure 6, the upper layer of RSIW can utilize an aperture-coupled feeding method. The H-plane T-junction power divider consisting of two layers of SIW is employed in this design. A one-to-two power divider network is placed on the lower layer, while the upper layer sequentially feeds two radiation slots through a single coupling path, then eight slots can be equally fed. Additionally, due to the higher cutoff frequency of SIW than that of RSIW, which can cause the different element spacing after array formation. To avoid this, the width of the lower SIW layer is kept similar to that of the upper RSIW by selecting an I-shaped slot for energy coupling.

The antenna is connected to a 50-Ω coaxial line via SMPM connectors. Energy is fed through the lowermost port, transformed from quasi-TEM mode to TE_{10} mode in the waveguide via a GCPW-SIW transition. The lowermost five layers of dielectric substrate are set with a thickness of h_3. The lowermost metal layer serves as a ground for the middle SIW layer, on which an I-shaped slot is etched for energy coupling. The middle five layers of dielectric substrate is set with thickness of h_2, and the middle metal layer serves as the ground for the upper RSIW. Two straight slots are etched on the middle metal layer, to couple energy to the upper RSIW radiation slots. Table 2 provides the optimal dimension values for the GCPW-SIW-fed RSIW structure.

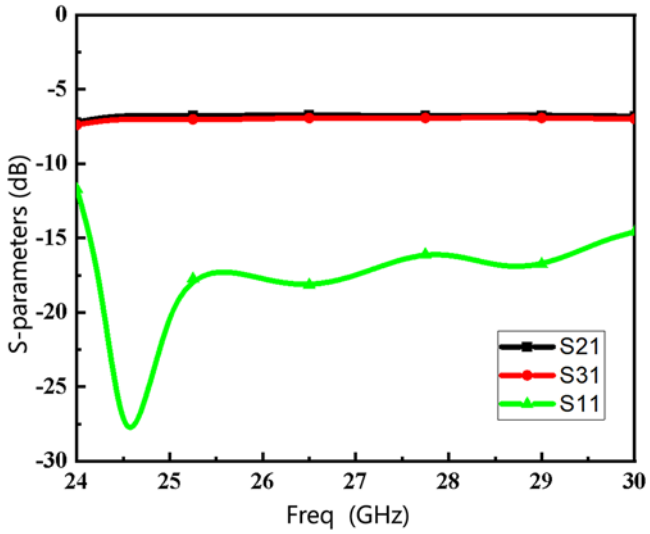


Figure 7. The simulated S-parameters of series-parallel SIW feeding network.

The simulated results of this two-layer (in bottom and middle layer) series-parallel SIW feeding network are presented in Figure 7, showcasing its S-parameters and transmission loss, showcasing its S-parameters and transmission loss. Evidently, this series-parallel combined feeding network exhibits wideband characteristics, with a −15 dB impedance bandwidth covering 24.25–29.5 GHz, fulfilling the design requirements for 5 G mmWave bands. Transmission loss within the operating band ranges from 6.63 to 7.03 dB/port, with a variation less than 0.5 dB. The simulated results indicate that GCPW-SIW-fed RSIW has good transmission properties and low loss.

https://doi.org/10.1017/S1759078725000534 Published online by Cambridge University Press

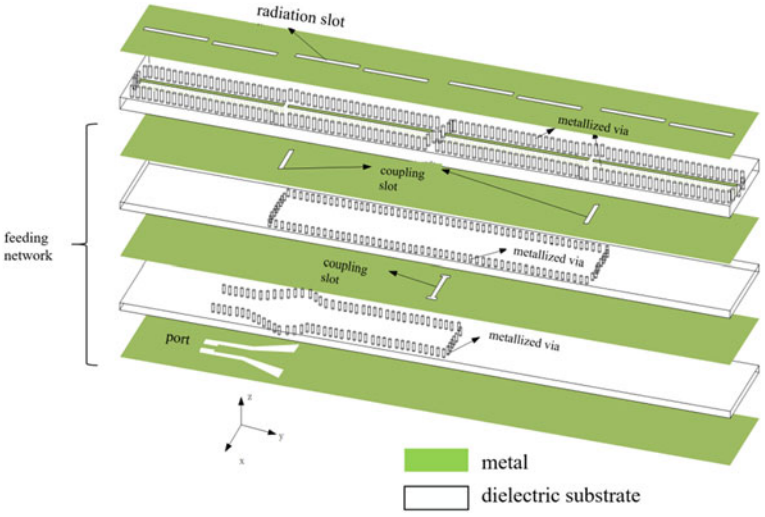


Figure 8. Exploded view of antenna subarray.

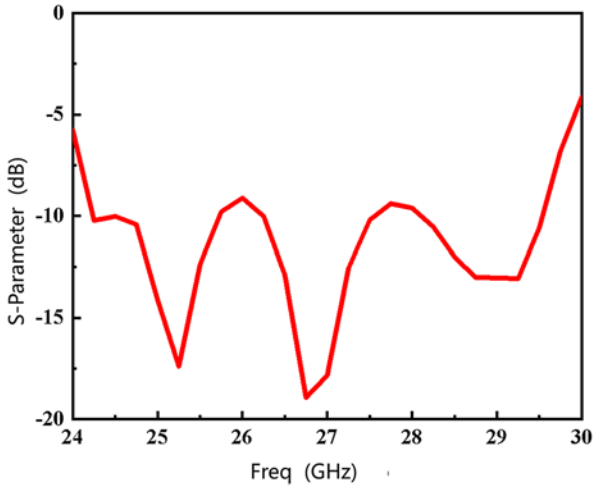


Figure 9. Simulated S_{11} of antenna subarray.

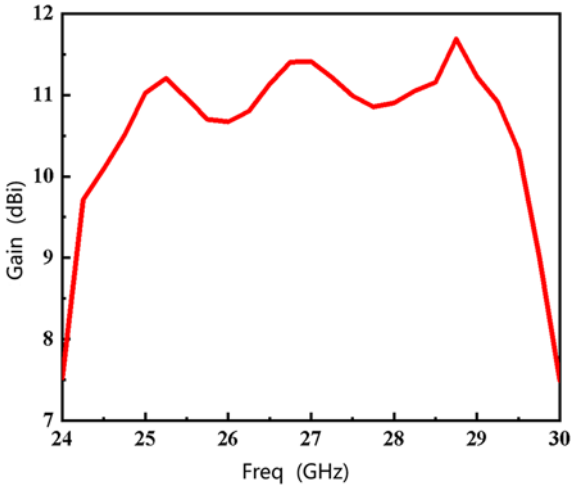


Figure 10. Simulated gain of antenna subarray.

Assembly of antenna subarray

The optimized radiation section is connected to the feeding network, and the three-dimensional schematic of the overall structure is shown in Figure 8. The performance is simulated and optimized using ANSYS HFSS. As can be seen from Figure 9, the antenna subarrays cover an operating bandwidth of 24.25–29.5 GHz, with an absolute bandwidth of 5.25 GHz and a relative bandwidth of ~20% for VSWR less than 2.

Figure 10 shows the gain variation in the 0° direction within the operating bandwidth of the antenna subarray. It can be seen that the gain variation within the operating bandwidth is stable, with a minimum of 10 dBi and a maximum of 11.5 dBi of gain. Figure 11 presents the E-plane radiation patterns at 24.25, 27, and 29.5 GHz. It can be observed that the overall radiation performance of the antenna subarray with the feeding network remains stable, with a beamwidth above 106° for each element. The minimum beamwidth is 106° at the low-frequency point of 24.25 GHz, and the maximum beamwidth is 124° at the high-frequency point of 29.5 GHz.

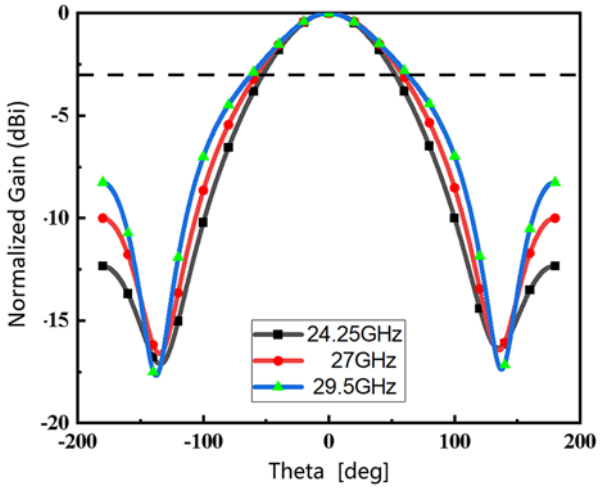


Figure 11. Normalized radiation patterns of the antenna subarray at 24, 25, 27, and 29.5 GHz.

https://doi.org/10.1017/S1759078725000534 Published online by Cambridge University Press

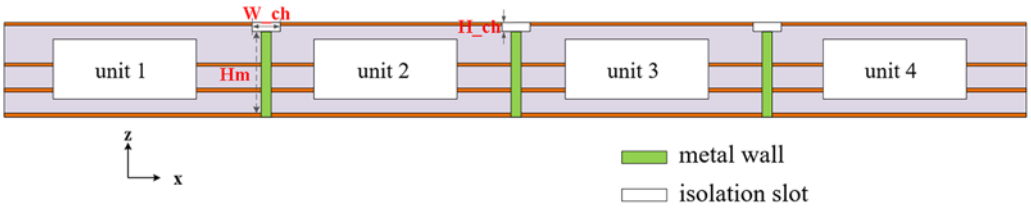


Figure 12. Side view of the antenna array.

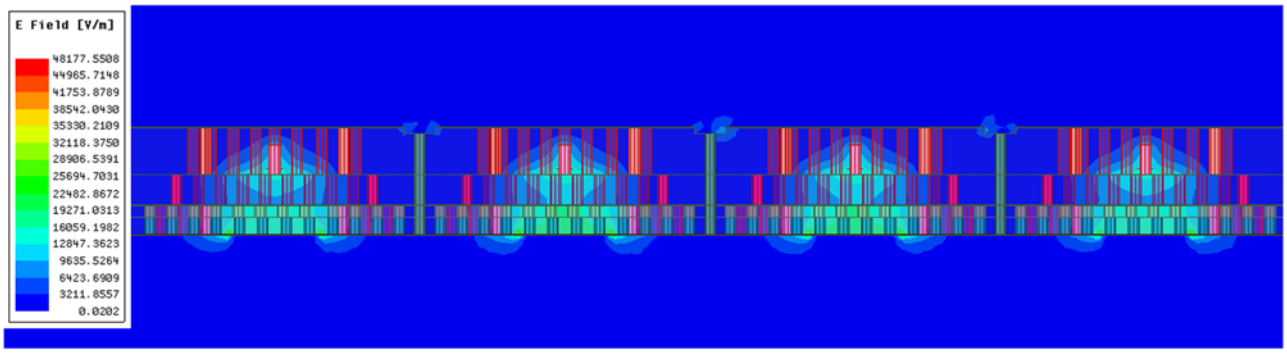


Figure 13. Electric field distribution on the scanning plane XOZ at 27 GHz.

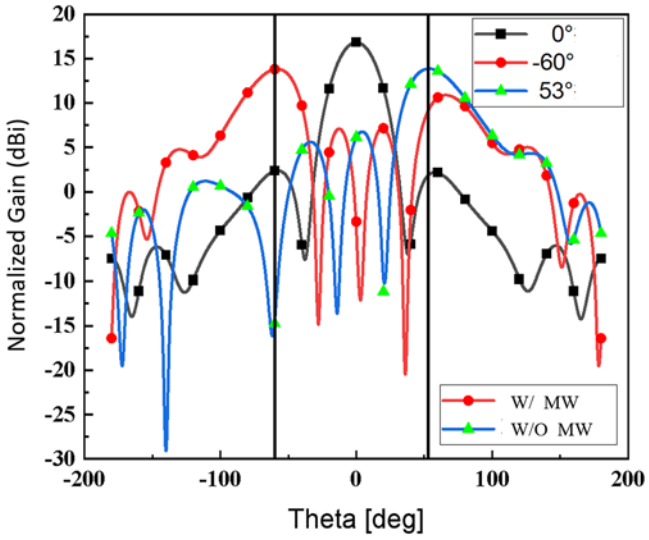


Figure 14. Impact of the metal vias on the scanning performance of the antenna array.

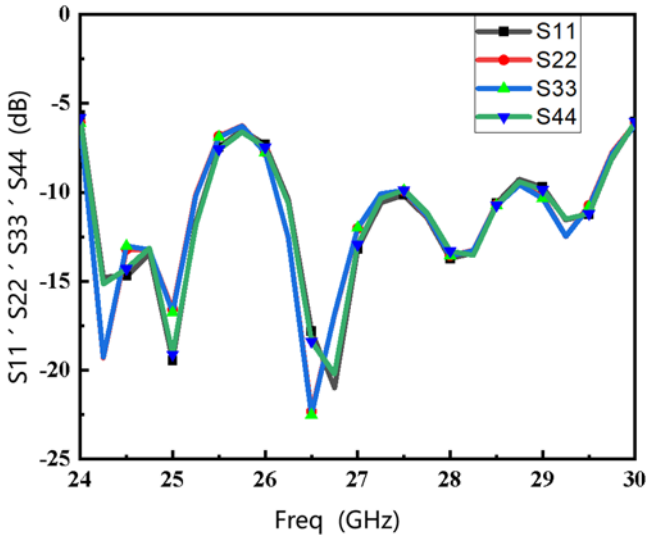


Figure 15. Simulated reflection coefficient of the antenna array.

Assembly of phased array antenna

The designed subarrays are equally spaced in line to form a four-element array, and the array structure is shown in Figure 12. As observed from the simulation, when the element spacing exceeds a certain threshold, grating lobes may appear, and element spacing affects the level of side lobes continuously. Larger element spacing can lead to higher side lobe levels, which can cause unwanted radiation in non-main beam directions, reducing the efficiency of the main beam. To avoid grating lobes during scanning, the element spacing should be less than $0.53\lambda_0$, which is finally optimized as $0.412\lambda_0$. The overall dimension of the array antenna is $1.68 \times 3.136 \times 0.15\lambda_0$ @ 26.875 GHz.

The phased array radiation pattern is influenced by both the element factor and the array factor. Scanning performance can be improved by enhancing inter-element isolation. Removing a piece of metal between elements on the ground plane of the RSIW, to block electromagnetic waves from propagating in the form of surface waves can reduce inter-element coupling and improve isolation. Furthermore, the physical barriers such as metal walls and isolation slots can easily be added between elements to block electromagnetic wave propagation through the substrate, thereby reducing coupling. The dimensions of the designed antenna are given as follow. The width of the isolation slot W_ch is 0.5 mm, and the depth of the excavated dielectric substrate H_ch is 0.094 mm. The height of the metal wall under the isolation slot H_m is 1.598 mm. The electric field distribution on the scanning plane of

https://doi.org/10.1017/S1759078725000534 Published online by Cambridge University Press

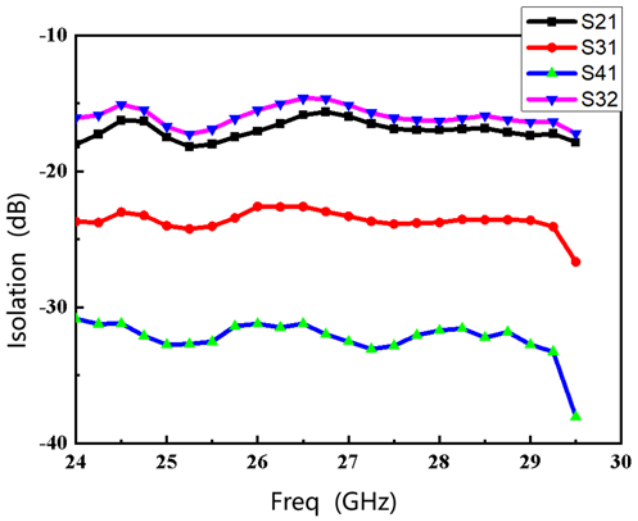


Figure 16. Simulated isolation between elements of the antenna array.

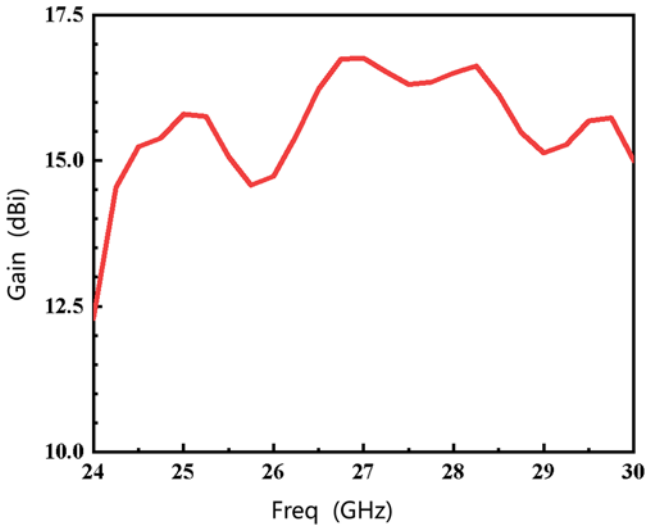


Figure 17. Simulated gain of the antenna array.

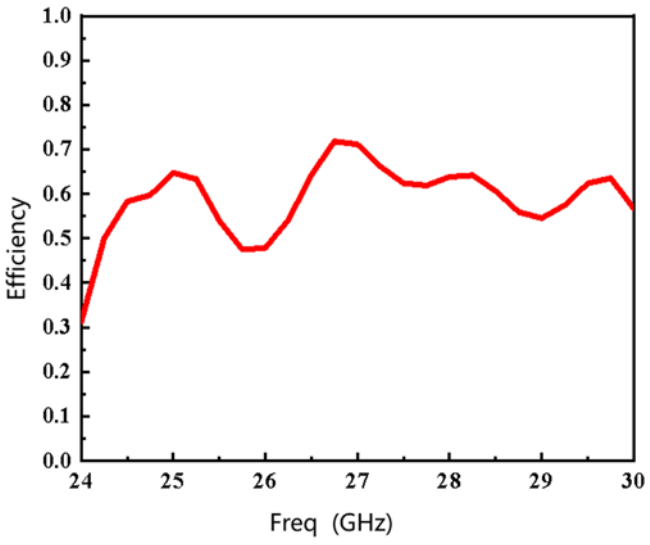


Figure 18. Simulated efficiency of the antenna array.

the array antenna is shown in Figure 13. As can be seen, most of the fields reside between the ridge and the upper wall of the waveguides, and it is possible to observe greater concentration of electric field in region above the ridge. The electric field distribution within the cross section of the RSIW shows that the adoption of ridge can control the electric field distribution. Since the feeding network is SIW, the surrounding metal posts can well confine the energy, resulting in minimal mutual coupling between array elements after assembly. Except for a small amount of energy coupled in the form of surface waves, there is little energy coupling in the middle layers. Furthermore, block effect of isolation slots by removing a piece of metal can also be observed, reducing the coupling and improve isolation between the array elements.

As observed from optimization, after the assembly, the main factors affecting the scanning angle of the phased array lie in the depth of the isolation slot and the metallized via hole added under the isolation slot. Figure 14 shows the scanning patterns with and without metal vias under the isolation slot at 27 GHz. The maximum scanning angle with metal vias is ±60°, while the maximum scanning angle without a metal vias is only ±53°, with a difference of ±7° corresponding to a 3 dBi gain drop. It indicates that adding a metal vias improves isolation and array scanning performance, while the requirement of difference between the main lobe and the side lobes should be less than 3 dB is still satisfied.

Each port of the 1 × 4 array is excited with equal amplitude and in-phase excitation. As shown in Figure 15, the S_{11} covers most frequencies of 24.25–29.5 GHz. Figure 16 shows the isolation between adjacent ports of the antenna. The isolation of ports 12, 23, 31, and 41 can reach below −15 dB, exhibiting good coupling performance. Figure 17 shows the actual gain within the operating bandwidth is above ∼15 dBi, with the gains corresponding to the upper and lower limits of the operating frequency being 14.5 dBi @25.8 GHz and 16.8 dBi @ 27 GHz. Since the antenna adopts the series-parallel combined feeding network, that the stability of the radiation pattern is better than that of only series feeding. Figure 18 shows the efficiency of the antenna, which is above 50% within the frequency band.

Figure 19 presents the gain pattern on the scanning plane at 24.25, 27, and 29.5 GHz. It can be observed that the array antenna can achieve a minimum scanning range of ±55° and a maximum scanning range of ±62° within the operating bandwidth in the E-plane (Phi = 0 plane). As the phase increases, the scanning angle increases, and the gain drop is relatively smooth. At the lowest frequency of 24.25 GHz, the gain in the 0° direction is 14.7 dBi, there is no significant gain drop when scanning to ±20° and ±40°, the scanning angle corresponding to 3 dBi gain drop is ±62°. At the mid-frequency of 27 GHz, there is a slight gain drop when scanning to ±20° and ±40°, and the scanning angle corresponding to 3 dBi gain drop is ±58°. At the highest frequency of 29.5 GHz, there is still a slight gain drop when scanning to ±20° and ±40°, and the scanning angle corresponding to 3 dBi gain drop is ±55°. It can be seen that as the frequency increases, the antenna beam scanning always meets the specification requirement of a ±55° scanning angle for the four-element array within the operating bandwidth.

https://doi.org/10.1017/S1759078725000534 Published online by Cambridge University Press

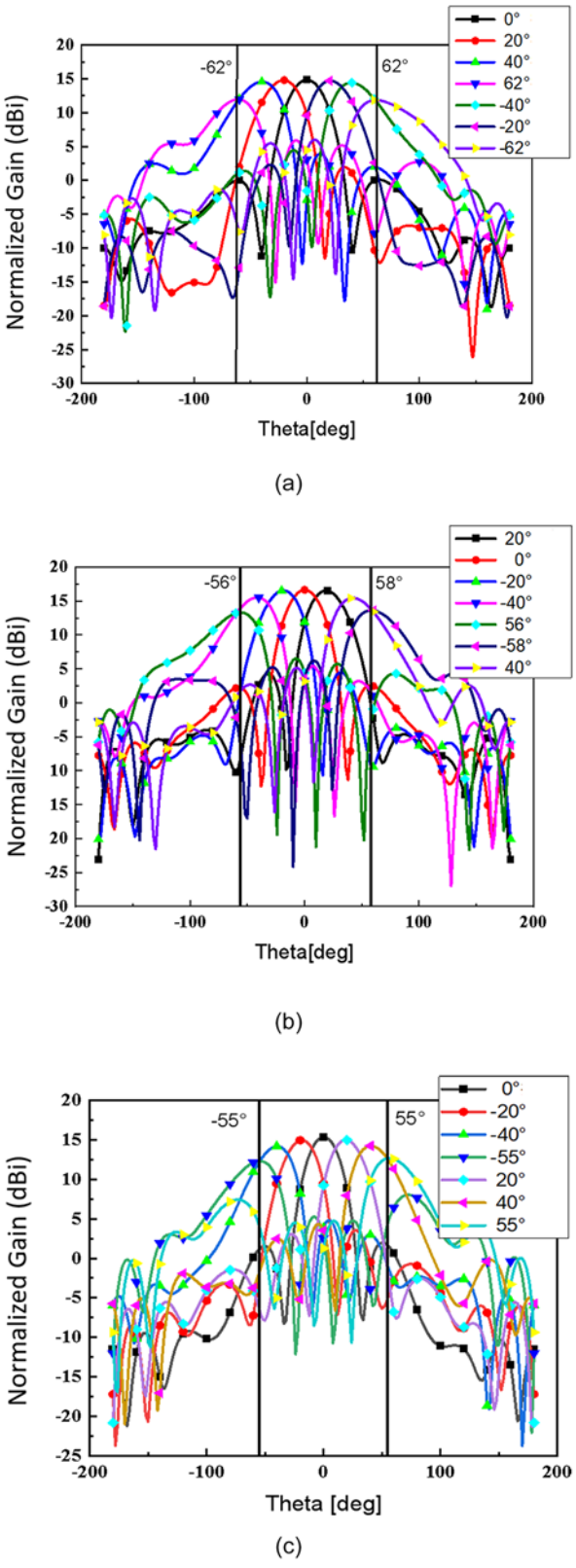


Figure 19. Scanning pattern of the antenna array in the XOZ plane at (a) 24.25 GHz, (b) 27 GHz, and (c) 29.5 GHz.

Measurement and results

The antenna array is fabricated and measured according to the proposed design to verify the performance. The fabrication is carried out using the LTCC process, with FerroA6M material for the substrate. The overall thickness of the antenna is 1.692 mm, consisting of 18 layers of 0.094 mm dielectric substrate. The fabricated prototype is shown in Figure 20. To prevent oxidation of the antenna metal, a layer of gold was plated on the metal surface of the antenna.

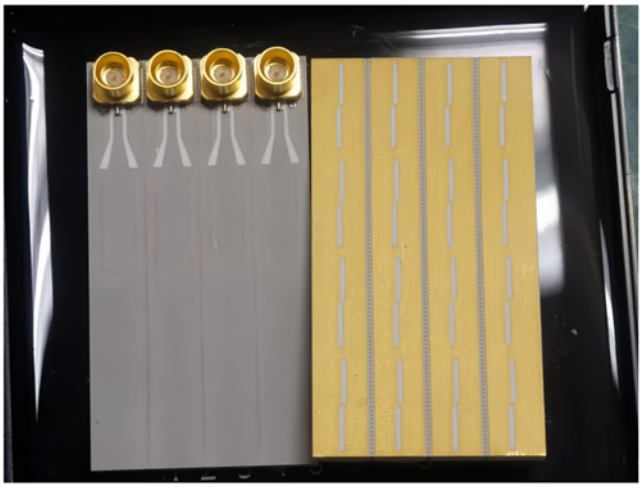


Figure 20. Prototype photograph of the fabricated phased array antenna.

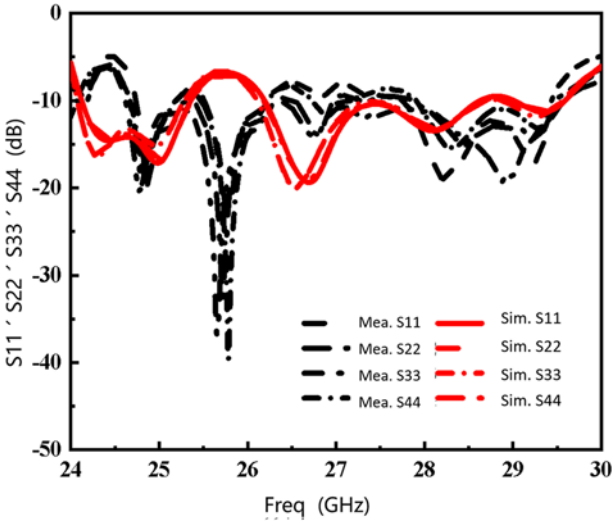


Figure 21. Simulated and measured results of S-parameters for each port of the antenna array.

The antenna array is connected to 2.92-mm SMPM connectors with a characteristic impedance of 50 Ω. The matching and radiation performance of the antenna were tested using a Vector Network Analyzer (R&S ZVA67 VNA) and a microwave anechoic chamber (MVG Satimo StarLab). Figure 21 presents the simulated and measured reflection coefficient for the four ports of the array antenna. It can be observed that the measured S_{11}, S_{22}, S_{33}, and S_{44} exhibit a consistent trend with their simulated results, with minor frequency deviations. These deviations are attributed to the influence of the actual test environment and the shrinkage of the LTCC substrate after processing, resulting in operating frequencies higher than simulated frequencies. The resonance point at low frequency is slightly lower than the simulated results, which may be

https://doi.org/10.1017/S1759078725000534 Published online by Cambridge University Press

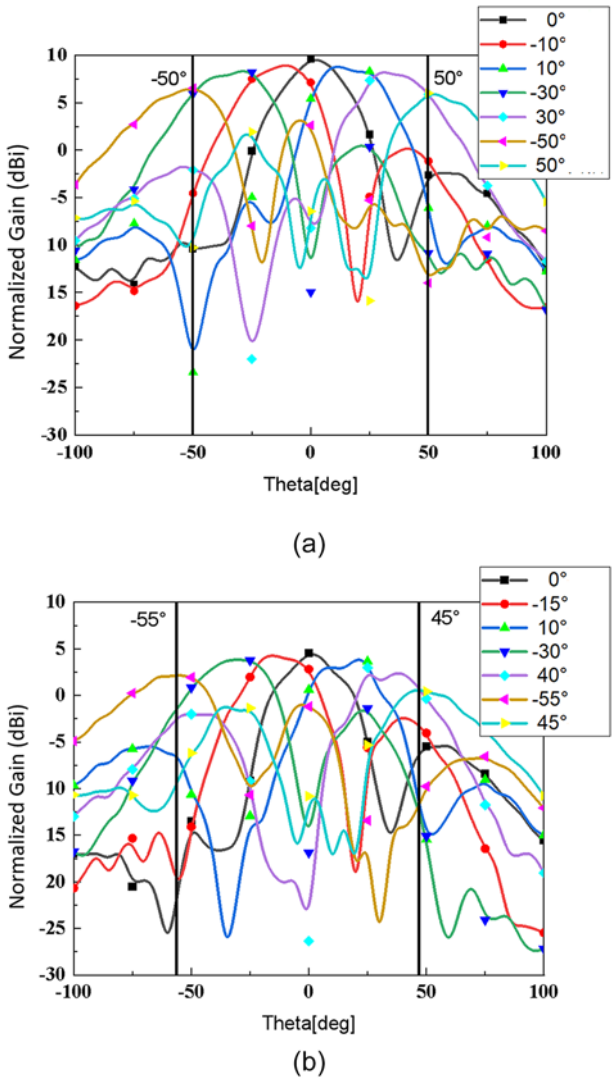


Figure 22. Measured scanning patterns of the antenna array XOZ-plane scan at (a) 27 GHz and (b) 29.5 GHz.

due to welding errors between the antenna and SMPM connector. These errors are within the normal range of variation.

Figure 22 (a) and (b) shows the continuous scanning patterns of the antenna's XOZ plane (E-plane) at frequency points of 27 and 29.5 GHz, respectively. The results reveal that the overall measured scanning angle is ±5° lower than the simulated results. At high frequencies, a shift is observed, and minor differences exist in both the pattern and gain values. These differences are partly due to processing and assembly errors and partly due to errors introduced by the test environment, but they are all within acceptable limits. Based on the above measurement, the performance of the antenna's simulation results is effectively validated.

Comparison and discussion

RSIW does not necessarily provide a wider scanning angle directly, but its narrow width is beneficial to wider the scanning range. RSIW is smaller in size than SIW at the same frequency, which means the spacing between two RSIW slot subarrays can be smaller than its SIW counterpart. The widest scanning range for phase array requires an element/a subarray spacing around 0.4 wavelength [18]. Since the width of SIW is about half wavelength, the spacing between two SIW slot subarrays cannot be smaller than 0.5 wavelength, the scanning range of the phase array based on SIW slot subarray is limited. On the hand, for phase array based on RSIW slot subarray, the spacing does not have this limitation; thus, the corresponding phase array can have wider scanning range.

Table 3 compares the proposed mmWave wideband high-gain phased array with its counterparts recently reported in papers [14, 16, 19–25]. Paper [19] features a similar inter-element spacing and higher peak gain, but the proposed antenna still achieves a broader scanning range. The proposed design operates within a ∼20% bandwidth at 24.25–29.5 GHz, which is comparable to the slotted SIW antennas in papers [21] and [14, 16, 25], both operating within a similar frequency range. However, the proposed antenna outperforms these counterparts in terms of bandwidth and peak gain, achieving a ∼20% bandwidth, and a peak gain of 14.5 dBi. This is notably higher than the 6% bandwidth and 11 dBi reported in paper [21]. At the same time, the inter-element spacing and scanning range is more desirable than reference [14, 16, 25]. When compared to the fixed-frequency antennas in papers [20, 22–24, 26], the proposed design demonstrates a clear advantage in terms of bandwidth, as these antennas are limited to specific frequencies without the wideband capabilities. Additionally, the proposed antenna's peak gain surpasses that of the 5.8–12.8 dBi range in papers [20, 22–24, 26], while maintaining a wider scanning range than in papers [20, 22, 24, 26]. In summary, the proposed slotted RSIW antenna exhibits satisfied performance in terms of wide operating bandwidth, broad scanning range, and high peak gain compared to its counterparts.

This design can be implemented using different multi-layer planar circuit processes, and both LTCC and HDI process are suitable to the design. Although LTCC is adopted in this work and the design based on it has good performance of high radiation efficiency due to the low-loss substrate material, its mass production is costly. The efficiency of the design based on HDI process is relatively poorer, mainly due to the high loss of substrate material, but its mass production cost is quite low. Therefore, HDI can also be adopted to expand the scope of design.

Several limitations still exist. First, regarding the design of the slot antenna subarray, the slot structure is not perfectly symmetrical. This asymmetry affects the cross-polarization level to a certain extent after array assembly. Second, the scanning range is still limited, which less than ±60°a generally requirement for many mmWave terminal applications. Lastly, the adoption of SIW as the transmission line results in relatively high costs and complicated feeding network. Therefore, for future work, research will be carried out on the designing of colinear slot array to solve cross-polarization, broadening the unit beamwidth to enhance the scanning coverage of the phased array antenna. Moreover, improvement on the feeding network, for example reduction of number of feed layers should also be carefully considered.

Conclusion

In this paper, a novel RSIW slot mmWave beam-scanning phased arrays is proposed. The antenna array adopts staggered slot radiating elements and incorporates additional radiation elements on the non-scanning plane to enhance the gain. The LTCC process enables the RSIW slot antenna array to achieve wideband transmission and increasing half-power beamwidth above 106° for the corresponding element. The series-parallel combined

https://doi.org/10.1017/S1759078725000534 Published online by Cambridge University Press

Table 3. Performance comparisons with other reported beam-scanning antennas

Ref.	Structure type	Operating bandwidth	3-dB scanning range	Peak gain	Inter-elements spacing/No. of element	Polarization
[19]	Slotted RSIW	9.7–10.3 GHz (6%)	±45°	20 dBi	$0.46\lambda_0/1 \times 8$	Linear
[20]	RSIW	12.1 GHz (Fixed-frequency)	−48° to 42°	12.8 dBi	NA/1 × 1	Linear
[21]	Slotted SIW	24–26 GHz (6%)	±56°	11 dBi	NA/1 × 1	Linear
[22]	Slotted SIW	2.6 GHz (Fixed-frequency)	−31° ~ 41°	9.2 dBi	NA/1 × 1	Linear
[23]	Slotted SIW	5.0 GHz (Fixed-frequency)	−60° ~ 65°	11.8 dBi	NA/1 × 1	Linear
[24]	Slotted SIW	5.8 GHz (Fixed-frequency)	34° ~ 59°	12.4 dBi	NA/1 × 1	Linear
[26]	Slotted SIW	4.5 GHz (Fixed-frequency)	40.66° ~ 31.32°	5.8 dBi	NA/1 × 1	Linear
[16]	SIW Horn	27.5–29.5 GHz (5.3%)	±44°	8.1 dBi	$0.5\lambda_0/1 \times 4$	Dual LP
[14]	Slotted SIW	25.8–28.8 GHz 11%)	±44°	10.2 dBi	$0.52\lambda_0/1 \times 4$	Dual LP
[25]	SIW	24.2–27.85 GHz (11.3%)	±41°	9.2 dBi	$0.61\lambda_0/1 \times 4$	Dual LP
This work	Slotted RSIW	24.25–29.5 GHz (20%)	±62° (24.25 GHz) ± 58° (27 GHz) ± 55° (29.5 GHz)	14.5 dBi	$0.41\lambda_0/1 \times 4$	Linear

feeding network further enhanced the wideband and low loss characteristics of the slot antenna array. By adding isolation slots and metal vias between adjacent array elements, energy coupling between array elements is reduced, further improving isolation below −15 dB and improving scanning angle up to ±7°. As a result, the array exhibits exceptional beam-scanning proficiency with a wide bandwidth of ~20%, featuring a maximum scanning angle spanning ±62° with minimal gain variations. Throughout this entire operating bandwidth, the scanning angles reaching up to ±55°, and the gain is above 14.5 dBi. The element spacing is finally optimized as $0.41\lambda_0$, and the overall dimension of the array antenna is $1.68 \times 3.136 \times 0.15\lambda_0$, which is formed in compact LTCC package. These features show antenna array proposed can be applied to mmWave communication systems.

Funding statement. This work was supported in part by the National Natural Science Foundation of China under Grant 62371141, 62271212, and in part by Guangdong Basic Applied Basic Research Foundation Grant Outstanding Youth Fund Project under Grant 2021B1515020039.

Competing interests. The authors declare that they have no known competing financial interests or personal relationships that could have appeared to influence the work reported in this paper.

References

1. **Hong W, Baek K-H and Ko S** (2017) Millimeter-wave 5G antennas for smartphones: Overview and experimental demonstration. *IEEE Transactions on Antennas and Propagation* **65**(12), 6250–6261.
2. **Hirokawa J** (2016) Millimeter-wave antenna technologies for 5G mobile communication systems. *Proceedings IEEE International Workshop on Electromagnetics: Applications and Student Innovation Competition (iWEM)*, 1–3. https://doi.org/10.1109/iwem.2016.750492
3. **Andrews JG, Buzzi S, Choi W, Hanly SV, Lozano A, Soong AC and Zhang JC** (2014) What will 5G be? *IEEE Journal on Selected Areas in Communications* **32**(6), 1065–1082.
4. **Qu Z, Qu S-W, Zhang Z, Yang S and Chan CH** (2020) Wide-angle scanning lens fed by small-scale antenna array for 5G in millimeter-wave band. *IEEE Transactions on Antennas and Propagation* **68**(5), 3635–3643.
5. **Gu X, Liu D and Sadhu B** (2021) Packaging and antenna integration for silicon-based millimeter-wave phased arrays: 5G and beyond. *IEEE Journal of Microwaves* **1**(1), 123–134.
6. **Gao H, Wang W, Fan W, Zhang F, Wang Z, Wu Y, Liu Y and Pedersen GF** (2021) Design and experimental validation of automated millimeter-wave phased array antenna-in-package (AiP) experimental platform. *IEEE Transactions on Instrumentation and Measurement* **70**, 1–11.
7. **Kavitha L and Raglend IJ** "A wide-scan phased array antenna for a small Active Electronically Scanned Array: A review", Circuits, Power and Computing Technologies (ICCPCT), 2013 International Conference on, 2013.
8. **Bozzi M, Pasian M, Moscato S, Moro R and Perregrini L** (2015) Two-material ridge substrate integrated waveguide for ultra-wideband applications. *IEEE Transactions on Microwave Theory & Techniques* **63**(10), 3175–3182.
9. **Kazemi R and Fathy AE** (2014) Design of single-ridge SIW power dividers with over 75% bandwidth. *EEE MTT-S International Microwave Symposium (IMS2014)*, 1–3.
10. **Kazemi R and Fathy AE** (2014) UWB 4-element ridge-SIW vivaldi antenna array. IEEE *Antennas & Propagation Society International Symposium (APSURSI)*, 1039–1040.
11. **Ding Y and Wu K** (2009) A 4*4 ridge substrate integrated waveguide (RSIW) slot array antenna. *IEEE Antennas and Wireless Propagation Letters* **8**, 561–564.
12. **Wang W, Zhong SS, Zhong YM and Liang XL** (2006) A broadband slotted ridge waveguide antenna array. *IEEE Transactions on Antennas and Propagation* **54**(8), 2416–2420.
13. **Zhong SS, Wang W and Liang XL** (2005) Compact ridge waveguide slot antenna array fed by convex waveguide divider. *Electronics Letters* **41**(21), 1151–1152.
14. **Liu W and Yan S** (2022) A design of millimeter-wave dual-polarized SIW phased array antenna using characteristic mode analysis. *IEEE Antennas and Wireless Propagation Letters* **21**(1), 29–33.
15. **Sun L, Li Y and Zhang Z** (2022) Wideband dual-polarized endfire antenna based on compact open-ended cavity for 5G mm-wave mobile phones. *IEEE Transactions on Antennas and Propagation* **70**(3), 1632–1642.
16. **Zhang J, Zhao K, Wang L, Zhang S and Pedersen GF** (2020) Dual polarized phased array with end-fire radiation for 5G handset applications. *IEEE Transactions on Antennas and Propagation* **68**(4), 3277–3282.
17. **Moreno RM, Ala-Laurinaho J, Khripkov A, Ilvonen J and Viikari V** (2020) Dual-polarized mm-wave endfire antenna for mobile devices. *IEEE Transactions on Antennas and Propagation* **68**(8), 5924–5934.
18. **Stutzman WL and Thiele GA** (2012) *Antenna Theory and Design*. John Wiley & Sons.
19. **Mallahzadeh A and Mohammad-Ali-Nezhad S** (2015) A low cross-polarization slotted ridged SIW array antenna design with mutual coupling

considerations. *IEEE Transactions on Antennas and Propagation* **63**(10), 4324–4333.

20. **Wei ZL, Wang S, Liu S, Li S and Wang J** (2023) Ku/Ka dual-band shared-aperture leaky-wave antenna with fixed-frequency and wide-angle beam scanning based on ridged SIW. *IEEE Transactions on Antennas and Propagation* **71**(5), 4558–4563.
21. **Serhsouh I, Himdi M and Lebbar H** (2020) design of coplanar slotted SIW antenna arrays for beam-tilting and 5G applications. *IEEE Antennas and Wireless Propagation Letters* **19**(1), 4–8.
22. **Ji Y, Ge L, Wang J, Chen Q and Wu W** (2019) Simple Beam Scanning SIW cavity-backed slot antenna using postloaded varactor. *IEEE Antennas and Wireless Propagation Letters* **18**(12), 2761–2765.
23. **Li Z, Guo YJ, Chen S-L and Wang J** (2019) A period-reconfigurable leaky-wave antenna with fixed-frequency and wide-angle beam scanning. *IEEE Transactions on Antennas and Propagation* **67**(6), 3720–3732.
24. **Lou T, Yang -X-X, Qiu H, Luo Q and Gao S** (2019) Low-cost electrical beam-scanning leaky-wave antenna based on bent corrugated substrate integrated waveguide. *IEEE Antennas and Wireless Propagation Letters* **18**(2), 353–357.
25. **Lu R, Yu C, Zhu Y and Hong W** (2020) Compact millimeter-wave end-fire dual-polarized antenna array for low-cost multibeam applications. *IEEE Antennas and Wireless Propagation Letters* **19**(12), 2526–2530.
26. **Chen K, Zhang YH, He SY, Chen HT and Zhu GQ** (2019) An electronically controlled leaky-wave antenna based on corrugated SIW structure with fixed-frequency beam scanning. *IEEE Antennas and Wireless Propagation Letters* **18**(3), 551–555.

https://doi.org/10.1017/S1759078725000534 Published online by Cambridge University Press